Oesinghaus L, Schlipf J, Giesbrecht N, Song L, Hu Y, Bein T, Docampo P, Müller-Buschbaum P.

Toward Tailored Film Morphologies: The Origin of Crystal Orientation in Hybrid Perovskite Thin Films.

***Advanced Materials Interfaces* 2016, 3(19)**

Advanced Materials Interfaces

Towards Tailored Film Morphologies: The Origin of Crystal Orientation in Hybrid Perovskite Thin Films

--Manuscript Draft--

Manuscript Number:	admi.201600403R1
Full Title:	Towards Tailored Film Morphologies: The Origin of Crystal Orientation in Hybrid Perovskite Thin Films
Article Type:	Full Paper
Section/Category:	
Keywords:	thin film structure; GIWAXS; sequential deposition; conversion mechanisms; perovskite solar cell
Corresponding Author:	Peter Müller-Buschbaum, Prof. Technische Universität München Garching, GERMANY
Additional Information:	
Question	**Response**
Corresponding Author Secondary Information:	
Corresponding Author's Institution:	Technische Universität München
Corresponding Author's Secondary Institution:	
First Author:	Lukas Oesinghaus
First Author Secondary Information:	
Order of Authors:	Lukas Oesinghaus
	Johannes Schlipf
	Nadja Giesbrecht
	Lin Song
	Yinghong Hu
	Thomas Bein
	Pablo Docampo
	Peter Müller-Buschbaum, Prof.
Order of Authors Secondary Information:	
Abstract:	Efficient perovskite solar cells can be produced by a wide variety of different methods. Previous results show that controlling the film morphology is critical to enhance the efficiency of the prepared devices. Here, we use grazing-incidence wide-angle X-ray scattering (GIWAXS) to study the morphology and especially the orientation distribution of CH3NH3PbI3 (MAPI) perovskite films prepared by five typical methods. We find that the investigated one-step methods produce non-oriented films, while the two-step deposition methods produce varying degrees of orientation depending on the method chosen to convert the highly oriented PbI2 precursor, providing direct evidence for different perovskite conversion mechanisms. At the example of one of the two-step methods we show that the morphology and crystal orientation of MAPI films is tunable by variation of the spin-coating temperature and by adding chloride to the conversion solution. By relating the precursor morphology to the resulting MAPI film morphology, the found preferential orientations are linked to specific conversion mechanisms, thereby establishing GIWAXS as an important tool towards a rational development of new synthesis methods.

WILEY-VCH

DOI: 10.1002/ ((please add manuscript number))
Article type: Full Paper

Towards Tailored Film Morphologies: The Origin of Crystal Orientation in Hybrid Perovskite Thin Films

*Lukas Oesinghaus, Johannes Schlipf, Nadja Giesbrecht, Lin Song, Yinghong Hu, Thomas Bein, Pablo Docampo *, Peter Müller-Buschbaum **

Lukas Oesinghaus, Johannes Schlipf, Lin Song, Prof. Peter Müller-Buschbaum
Physik-Department, Technische Universität München, Lehrstuhl für Funktionelle Materialien, James-Franck-Str. 1, 85748 Garching, Germany
E-mail: muellerb@ph.tum.de

Nadja Giesbrecht, Yinghong Hu, Prof. Thomas Bein, Prof. Pablo Docampo
Department of Chemistry, LMU München, Physical Chemistry and Nanoscience, Butenandtstr. 11, 81377 München, Germany
E-mail: pablo.docampo@cup.uni-muenchen.de

Keywords: thin film structure, GIWAXS, sequential deposition, conversion mechanisms, perovskite solar cell

Efficient perovskite solar cells can be produced by a wide variety of different methods. Previous results show that controlling the film morphology is critical to enhance the efficiency of the prepared devices. Here, we use grazing-incidence wide-angle X-ray scattering (GIWAXS) to study the morphology and especially the orientation distribution of $CH_3NH_3PbI_3$ (MAPI) perovskite films prepared by five typical methods. We find that the investigated one-step methods produce non-oriented films, while the two-step deposition methods produce varying degrees of orientation depending on the method chosen to convert the highly oriented PbI_2 precursor, providing direct evidence for different perovskite conversion mechanisms. At the example of one of the two-step methods we show that the morphology and crystal orientation of MAPI films is tunable by variation of the spin-coating temperature and by adding chloride to the conversion solution. By relating the precursor morphology to the resulting MAPI film morphology, the found preferential orientations are linked to specific conversion mechanisms, thereby establishing GIWAXS as an important tool towards a rational development of new synthesis methods.

1. Introduction

In recent years, perovskite solar cells based on methylammonium lead iodide ($CH_3NH_3PbI_3$ or MAPI) have gained increasing attention due to a rapid increase in power conversion efficiency from 3.9 % in 2009 to 20.8 % in 2016.[1,2] This rapid increase was possible due to the favorable material properties of MAPI. It has a band gap of roughly 1.5 eV, a large absorption coefficient, and can achieve large diffusion lengths of over 1 μm in polycrystalline thin films and more than 100 μm in single crystals.[3–6] These properties, in combination with the possibility of cheap device fabrication, the abundancy of its precursor materials and its potential environmental sustainability, make perovskite solar cells a promising challenger to existing solar cell technologies.[7,8]

Thin perovskite films for planar heterojunction solar cells are typically prepared by combining lead salts such as PbI_2, $PbCl_2$ or $Pb(CH_3COO)_2$ with organic cations such as methylammonium iodide (MAI) or methylammonium chloride (MACl). Deposition techniques can be classified into two categories, namely one-step methods, in which the precursors are mixed in the same solution with a common solvent, and two-step methods, in which the precursors are applied sequentially. One-step methods are usually faster, yet prone to yield inhomogeneous films.[9] The film quality is improved by a careful choice of precursors, solvent additives or solvent-engineering during or after deposition.[10,11] Two-step methods are generally more versatile: They usually start from an already crystalline precursor layer which is converted to the perovskite phase by exposing it to a solution or vapor containing the organic cation.[12–14] Having two independent fabrication steps allows for an easy inclusion or modification of additional treatment steps for improved efficiency.[15]

To gain a better understanding, a better control of the different methods for producing perovskite films and, thereby, higher device efficiencies, the crystal structures of the resulting

films as well as of the precursors must be studied in detail. Grazing-incidence wide-angle X-ray scattering (GIWAXS) is a versatile tool to analyze the morphology of thin films.[16] It has been used extensively to characterize thin polymer films for photovoltaic applications and has also already been employed to characterize the crystal structure of perovskite films.[17–21] Here, we give an overview over MAPI film morphologies produced by using a set of typical fabrication procedures investigated with scanning electron microscopy (SEM) and GIWAXS. In contrast to the investigated one-step methods, the two-step methods show drastically different morphologies and crystal orientations depending on the conversion method, evidencing fundamentally different conversion mechanisms. To understand the relationship of morphology and orientation between the precursor film and the resulting MAPI film depending on the conversion mechanism, we systematically tune the morphology of the precursor film by varying the spin-coating temperature and changing the chloride content of the conversion solution. Our results reveal that specific orientations in the MAPI films are the result of an in situ-conversion process, while others are the result of a dissolution-recrystallization process. Since this relationship is intrinsic to the crystal structures of lead iodide and MAPI, this study shows that GIWAXS is useful for an easy, rapid classification of the conversion mechanism of two-step methods starting from a crystalline lead iodide layer. Understanding the relationship between the different crystallization mechanisms and the chosen precursors is crucial for development of rationally designed film morphologies in perovskite thin films and ultimately reproducible photovoltaic device performance.

2. Examining Five Typical Film Deposition Methods

2.1. Sample preparation

For our study we compared five distinct methods, as presented schematically in **Figure 1**. We chose two one-step methods and three two-step methods to represent typical MAPI film

deposition techniques. All of these five methods have reached good device efficiencies.[11,14,22–24]

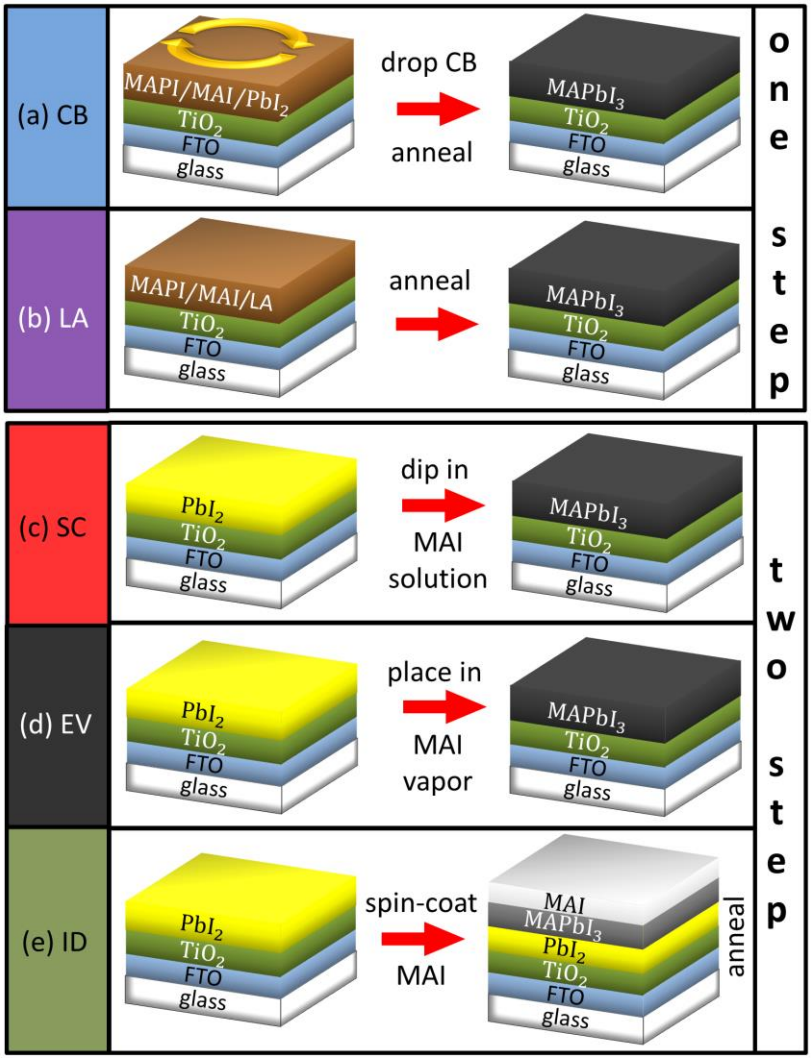

Figure 1. Overview over studied sample preparation methods named (a) chlorobenzene (CB), (b) lead acetate (LA), (c) solution conversion (SC), (d) evaporation (EV), and (e) interdiffusion (ID).

The investigated methods are the following: (a) A one-step method, in which 1:1 stoichiometric amounts of PbI_2 and MAI are dissolved in the common solvent DMF and spin-coated on a substrate. After a certain delay time, the anti-solvent chlorobenzene is dropped onto the spinning sample to induce fast crystallization of the MAPI phase, resulting in an extremely smooth and densely packed film.[11] Hereafter we refer to this as the chlorobenzene or CB method. (b) A one-step method, in which $Pb(CH_3COO)_2$ and MAI are spin-coated together in the common solvent DMF. The use of lead acetate leads to smoother, more

uniform films.[24] In this article we refer to this method as the lead acetate or LA method. (c) A two-step method, in which PbI_2 in DMF is spin-coated, and then converted into MAPI by immersing the sample in a mixed solution of MAI/MACl in 2-propanol,[22] hereafter referred to as the solution conversion or SC method. (d) A two-step method, in which PbI_2 in DMF is spin-coated and converted by placing it in MAI vapor,[23] hereafter referred to as the evaporation or EV method. (e) A two-step method, in which PbI_2 in DMF is spin-coated and converted by first spin-coating MAI in 2-propanol, leaving unreacted layers of PbI_2 and MAI, and then annealing the sample to let the MAI diffuse into the PbI_2 layer.[14] This method is hereafter referred to as the interdiffusion or ID method. We note that all the films prepared in this study fully cover the substrate and achieve good photovoltaic performances when employed in combination with TiO_2 and spiro-OMeTAD (cf. Figure S1).

2.2. Characterizing the morphology

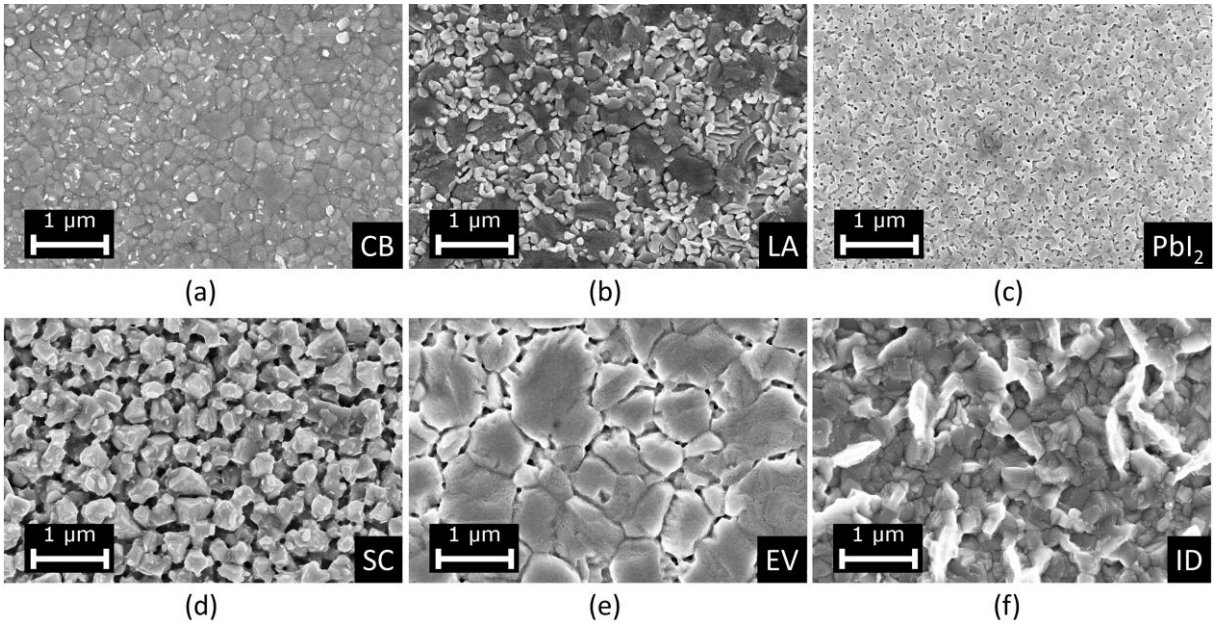

Figure 2. SEM top-view images of perovskite films fabricated with different methods: (a) chlorobenzene, (b) lead acetate, (c) PbI_2, (d) solution conversion, (e) evaporation, and (f) interdiffusion method.

Figure 2 shows SEM pictures of MAPI films prepared with the five different methods as discussed above. The one-step methods CB and LA produce dense films with low surface

roughness, while for the two-step methods we obtain a wider variety of surface morphologies. The PbI_2 precursor film used for all two-step methods has a smooth surface and pores which have an average size of roughly 40 nm. The SC method produces very rough films of individual crystallites of different sizes up to the micrometer range, while the evaporation method produces very flat films with large grains typically over 1 µm. The ID method produces very densely packed and overall rather flat films. Light transmission measurements show that all films absorb most of the light from 750 nm onwards with slight differences in transmission resulting from the fact that the investigated films vary in thickness as they are optimized for photovoltaic performance (cf. Figure S2).

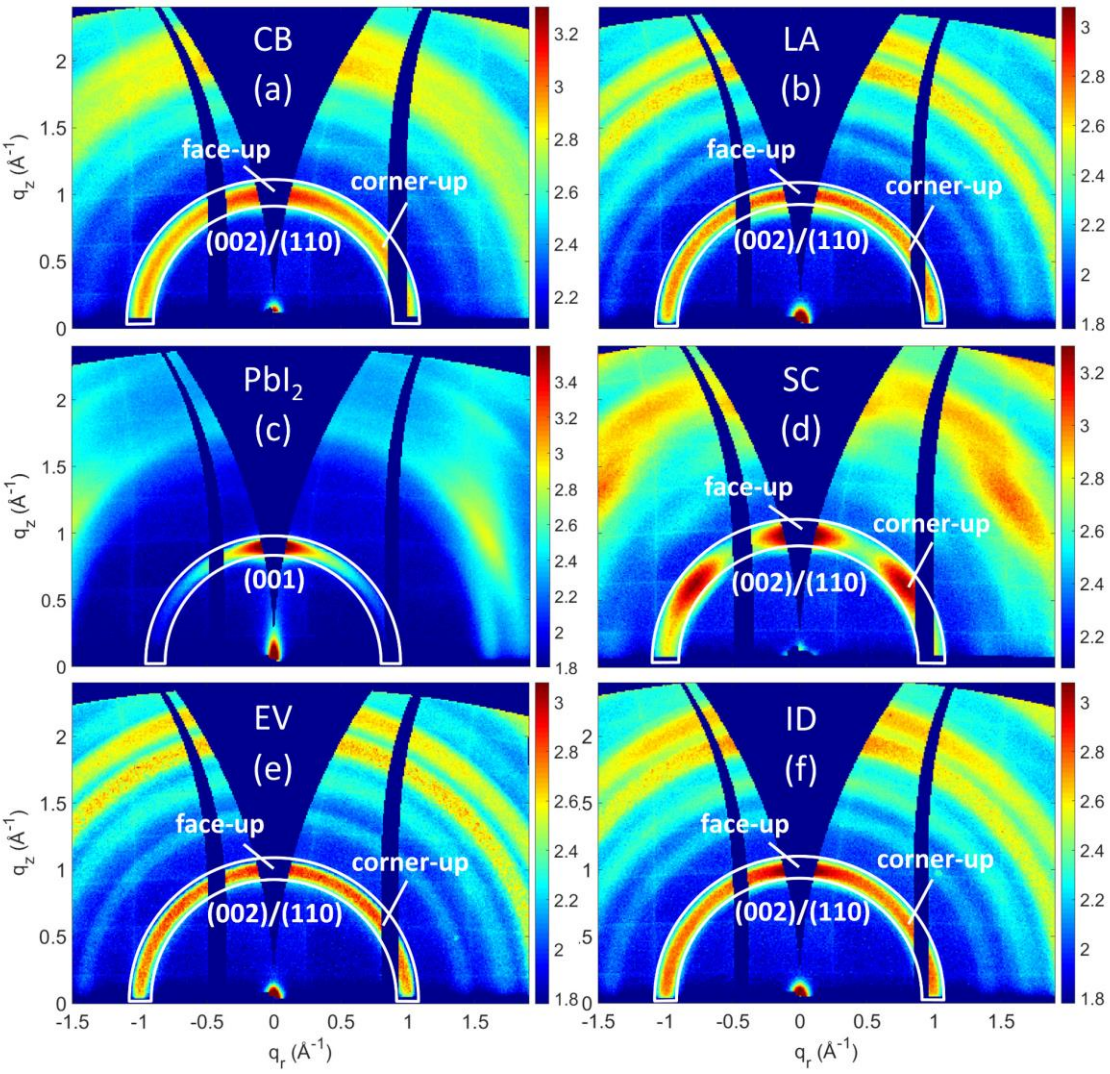

Figure 3. GIWAXS data of perovskite films fabricated with different methods: (a) chlorobenzene, (b) lead acetate, (c) PbI_2, (d) solution conversion, (e) evaporation, and (f) interdiffusion method.

In order to study the crystal structures of perovskite films, we performed GIWAXS measurements. In GIWAXS, the detector captures a two-dimensional slice through reciprocal space which allows the reconstruction of the crystal structure, where crystal plane spacing relates to the magnitude of the scattering vector, whereas the orientation of these planes, and thus of the crystallites, is apparent from the azimuthal intensity distribution.

Figure 3 shows 2D GIWAXS data for the five perovskite films plus the PbI_2 precursor layer used for the two-step methods. The component of the scattering vector perpendicular to the sample surface is q_z and $q_r = \sqrt{q_x^2 + q_y^2}$ is the in-plane component of the scattering vector parallel to the substrate. q is the total magnitude of the scattering vector and $\chi = \arctan\left(\frac{q_r}{q_z}\right)$ is the azimuthal angle. The azimuthal angle contains information of how scattering planes are tilted relative to the substrate. A (202) peak at 45° azimuthal angle, for example, would correspond to (202) crystal planes at an angle of 45° to the substrate. The conversion of the raw detector image to reciprocal space leads to the pixel-wise corrected intensity maps shown in Figure 3 with a wedge of missing information.[25] The origin of this missing wedge is the fixed incident angle in GIWAXS, unlike conventional X-ray diffraction (XRD), which leads to a non-negligible momentum transfer q_x in direction of the beam. Apart from the conversion to reciprocal space, a number of corrections, e.g. for beam polarization or detection efficiency, have to be applied to the raw detector picture to allow for a correct reconstruction of the reciprocal space morphology. A detailed explanation of the corrections and the reciprocal space conversion is given in the Supporting Information (SI).

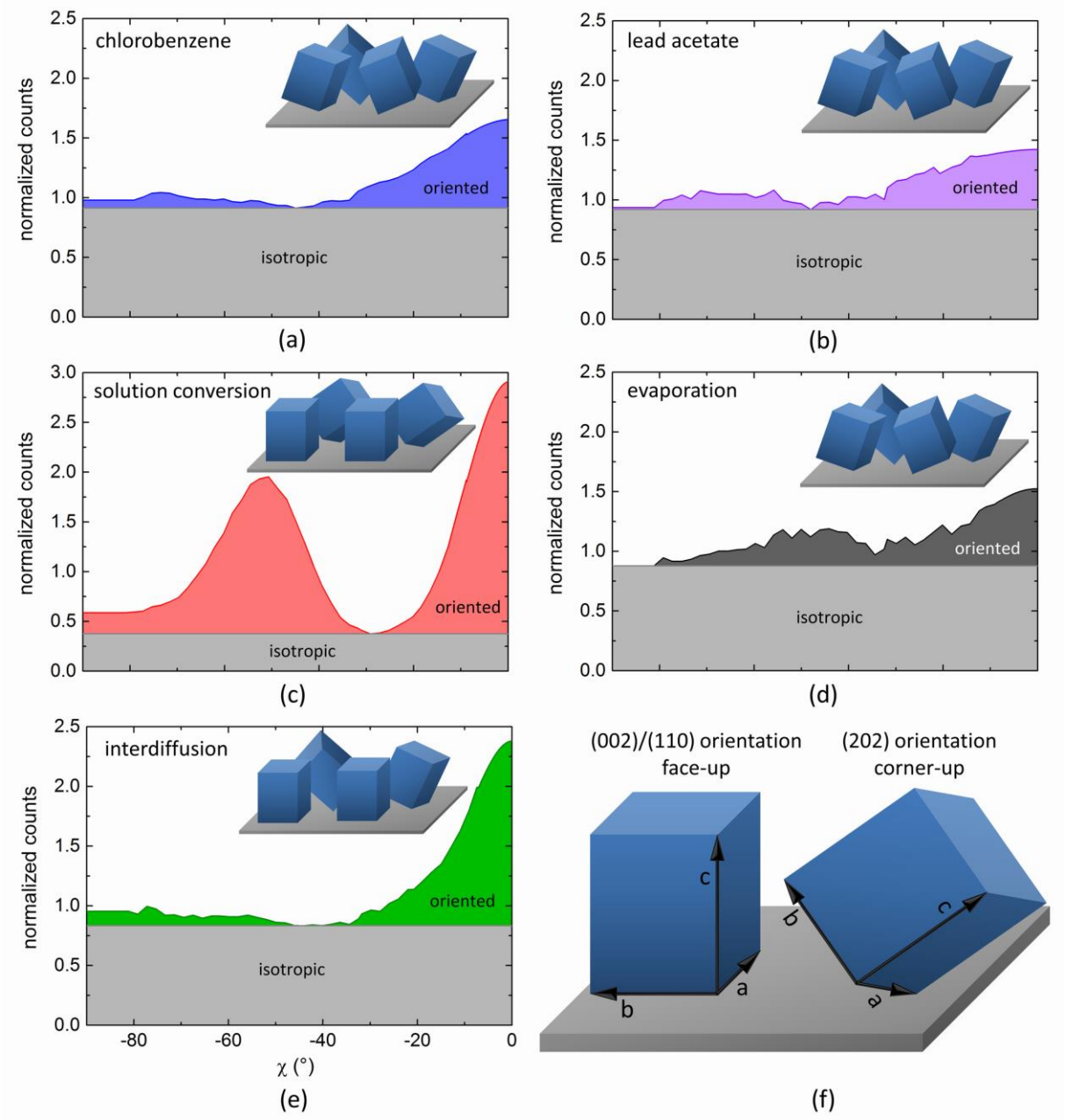

Figure 4. Azimuthal integration of the (002)/(110) peak from the GIWAXS data for perovskite films fabricated with different methods: (a) chlorobenzene, (b) lead acetate, (c) solution conversion, (d) evaporation and (e) interdiffusion method. The flat isotropic section of the distribution is grayed out. The different orientations are visualized on top in terms of a cubic MAPI crystallite. (f) Illustration of the two orientations found for a cubic crystallite.

To perform a quantitative analysis, we integrate the intensity along the azimuthal angle over the diffraction pattern arising from (002)/(110) planes which forms a Debye-Scherrer ring at about 1 $Å^{-1}$. This gives information about the orientation distribution of the crystal planes responsible for the (002)/(110) peak. The result is presented in **Figure 4**, where an amended

and normalized azimuthal integration of the (002)/(110) peak is shown (see SI for details on the data treatment) for all methods. To confirm our results, we compare with normalized XRD data (cf. Figure S3).

We evaluate the one-step methods first. Both, the CB and the LA sample, have a very flat azimuthal intensity distribution (cf. Figure 4 (a) and (b)) with no pronounced orientation peaks, but with a slight preference for (002)/(110) preferential orientation. As a simple estimation of the degree of orientation, we assign the flat part of the azimuthal integration to an isotropic orientation distribution of crystallites and the rest to oriented crystallites. Both samples have ~17% crystallites with preferential orientation. This measure of order does not consider the angular width of the orientations for samples with preferential orientation. It can be considered by looking at the azimuthal FWHM of the individual orientations. Due to its relative lack of orientation, we choose the CB sample as the reference for the XRD measurements. As expected from the GIWAXS data, the normalized XRD curves of the samples produced by the CB and LA methods are almost identical (cf. Figure S3 (b)). This lack of orientation can likely be seen as the norm for most perovskite films, making these methods suitable as a reference for other methods producing more oriented films. This is likely the result of the evaporation of the common solvent that leads to an increased concentration of the precursors, which in turn leads to precipitation close to the substrate thereby promoting random formation of nucleation centers for crystallization.

To evaluate the two-step methods, we first look at the orientation of the PbI_2 precursor film. Comparing the orientation of this precursor film to the orientation of the MAPI film yields information about the chemical and mechanical aspects of the conversion mechanisms. Chemically, the conversion can happen in-situ, i.e. by diffusion of the MAI into the PbI_2, hardly influencing the inorganic framework, or by dissolution-recrystallization, where the

inorganic lead cage is dissolved and recrystallized as MAPI.[26] Apart from the chemical conversion mechanism, crystallites can be moved or broken up mechanically by increasing crystal strain resulting from expansion of next neighbor Pb^{2+} distances during conversion.[27] PbI_2 has a layered structure in which lead layers are separated by iodide layers. The PbI_2 films prior to conversion show strong (001) preferential orientation (cf. Figure 3 (c) and Figure S4 (a)), meaning that the lead layers are lying parallel to the substrate. Nevertheless, all three two-step methods produce MAPI films with very different orientations, indicating that the conversion mechanism must be different.

The solution conversion method shows rather strong preferential orientation with 66% oriented crystallites (cf. Figure 4 (c)). There are two preferential orientations in the orientation distribution, one around a polar angle of 0° and one roughly around 55°. The 0° orientation corresponds to crystallites whose (002) or (110) planes are parallel to the substrate, i.e. face-up for a cube-shaped crystallite, and the 55° orientation corresponds to crystallites whose (202) planes are parallel to the substrate, i.e. corner-up for a cube-shaped crystallite (cf. Figure 4 (f)). Correspondingly, these two orientations show a larger intensity in the XRD for the solution conversion sample than for the chlorobenzene sample (cf. Figure S3 (c)). Because the film consists of individual crystallites with roughly cubic shape, these preferential orientations are also visible in the SEM image (cf. Figure 2 (d)). **Figure 5** shows the crystal structure of PbI_2, which can be seen as consisting of edge-sharing PbI_6 octahedra tilted 55° relative to the c-axis. In $MAPbI_3$, these octahedra are corner-sharing and parallel to the c-axis. Therefore, leaving the lead layers and the orientation of the PbI_6 octahedra intact during the conversion would result in (002)/(110) planes tilted 55° relative to the c-axis of the lead iodide, which is one of the preferential orientations we find for this method. Based on this relationship, we hypothesize that the corner-up crystallites are the result of a direct in-situ conversion. The face-up orientation has no such direct relationship to the crystals structure and orientation of the precursor film. One-step methods with preferential orientation tend to

produce (002)/(110) planes parallel to the substrate.[20,28,29] Therefore, we hypothesize that the (002)/(110) orientation is due to a dissolution-recrystallization process which competes with the in-situ conversion process producing (202) orientation.

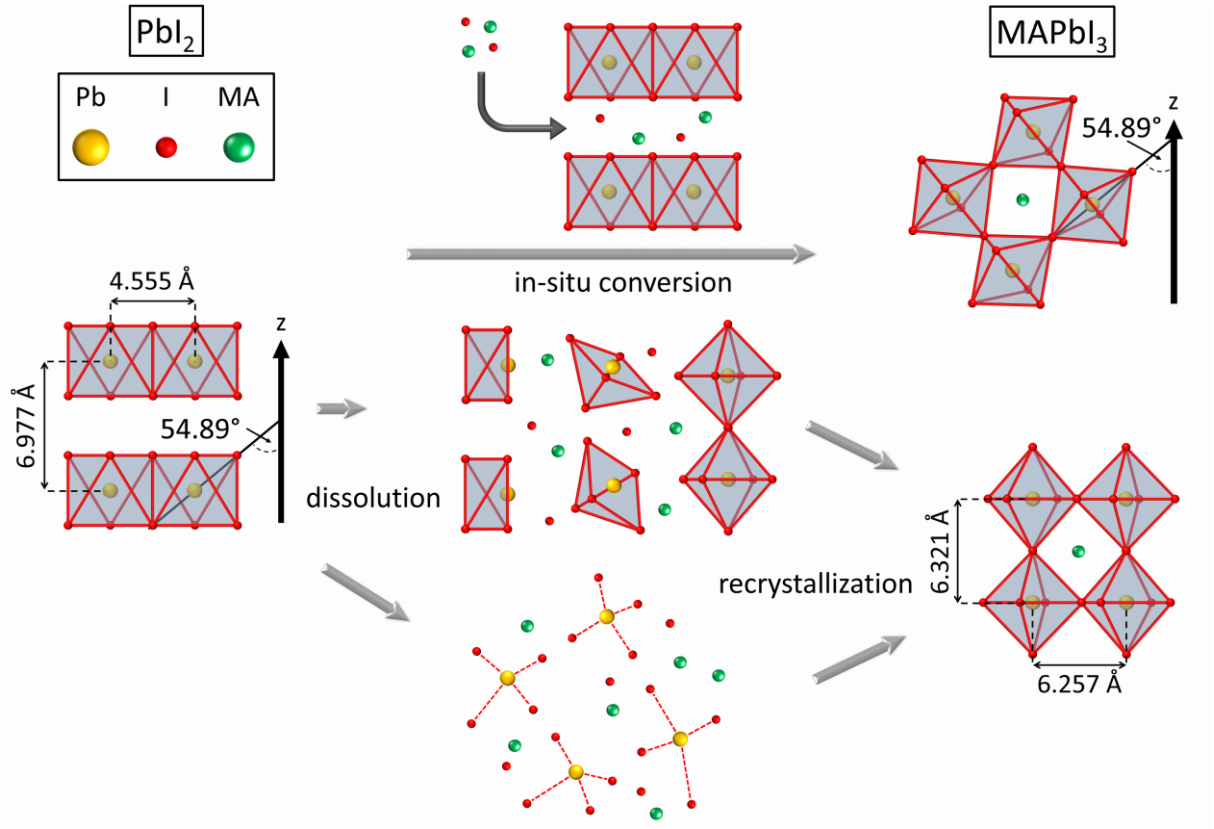

Figure 5. Visualization of the two general pathways for conversion of PbI_2 to MAPI in terms of PbI_6 octahedra.

The interdiffusion sample shows a reduced orientation with only 25% oriented crystallites (cf. Figure 4 (e)). There is one pronounced orientation in Figure 4 (e) at 0° azimuthal angle, meaning (002)/(110) preferential orientation, i.e. face-up orientation for a cube-shaped crystallite. We find a corresponding higher intensity of this peak in the XRD measurements (cf. Figure S3 (e)). As mentioned, this orientation was hypothesized to be due to a dissolution-recrystallization process which is to be expected for high MAI concentrations.[26] This seems to be at odds with the notion of diffusion of MAI into the PbI_2 film during the annealing process.[11] It is likely that only a thin layer on top is dissolved by the initial spin-coating of

the MAI that acts as a nucleation center for the crystals formed by the diffusion of MAI through this top layer. As most crystallites are not oriented, this seed layer is either not very oriented, which is probable due to fact that the dissolution of the PbI_2 film surface breaks the strong preferential orientation, or the seed layer picture is not a complete description of the conversion mechanism. Fully understanding the orientation distribution for this method requires further investigation.

For both the interdiffusion and the solution conversion method, we find a large number of non-oriented crystallites. As the volume of the film increases by a factor of about 1.7 during conversion from PbI_2 to $MAPbI_3$,[30] not all crystallites can remain in the same position, regardless of the chemical conversion mechanism. During the expansion, crystallites in the bulk break up into smaller crystallites, thereby possibly losing their orientation.[27] Furthermore, crystallites will have to be pushed out of the film during conversion, as most of the volume expansion occurs in-plane, due to the fact that the spacing between lead atoms for PbI_2 as compared to MAPI is much smaller within a lead layer, but similar between lead layers, i.e. along the direction perpendicular to the substrate (cf. Figure 5). Thus, part of the isotropic portion of the crystallite orientation distribution can be explained by mechanical reordering due to the volume expansion during conversion.

The evaporation sample has 19% oriented crystallites and no pronounced peaks, making it similar to the investigated one-step methods (cf. Figure 4 (d)), meaning that the strongly oriented PbI_2 film is converted into a completely non-oriented MAPI film. If there is a defined relationship between precursor orientation and MAPI film orientation, this would imply a reorganization of all PbI_6 octahedra, i.e. a dissolution-recrystallization process. Based on the intensity distribution in Figure 4, we would expect an XRD comparison similar to the lead acetate sample, with the XRD curves being almost identical. Instead, we find that peaks positions and intensities do not coincide, and the (211) peak is missing completely. A comparison to a simulation of alpha- and beta-MAPI powder shows that the evaporation

sample is cubic (cf. Figure S3 (a)). Pistor et al. found that a chloride content of less than 2% can lead to $MAPbI_{3-x}Cl_x$ assuming a cubic structure.[31] For the evaporation sample, no chloride was used in the fabrication, making its cubic structure surprising and hinting at further possible differences in the crystallization.

Due to the variety of different orientations found in the investigated two-step methods, in the following section we make use of the fact that the solution conversion sample shows both types of preferential orientation in order to conduct a systematic study on their origin.

3. The relationship between precursor morphology and MAPI film morphology

In order to prove that different orientations are the result of different conversion mechanisms, the morphology and orientation of the precursor film have to be varied and their influence quantified. For an in-situ conversion, a clear correlation between the degree of orientation of the precursor film and the MAPI film is to be expected. In-situ conversion should also be more likely in the absence of additives to the conversion solution and for flat and dense films, as a dissolution process should only happen at the interface with the conversion solution.[26] Following this line of thought, a dissolution-recrystallization mechanism would be more likely for porous films, and there is no reason to assume an obvious correlation of crystal orientations in the precursor and the perovskite film. It should be noted that (002)/(110) orientation is only a possible outcome of a recrystallization process, but not a necessary outcome. There is also a possibility of processes in between these two, e.g. a conversion by an intermediate phase as described by Moore et al. for a one-step process.[18] In such an intermediate process, a correlation between orientations might be present.

Because the solution conversion method produces both orientations that we wish to study and allows for an easy variation of fabrication parameters while still producing good films, we choose this method to study the correlation of precursor and MAPI film morphologies.

3.1. The influence of spin-coating temperature

The lead iodide film in two-step methods is often spin-coated at elevated temperatures, typically around 60 °C.[15,22,32] We studied lead iodide films spin-coated at three different temperatures (25 °C, 60 °C, 100 °C) and the resulting MAPI films produced by the solution conversion method to study the impact of the spin-coating temperature on the film morphology. (Details on the sample preparation can be found in the Experimental Details.)

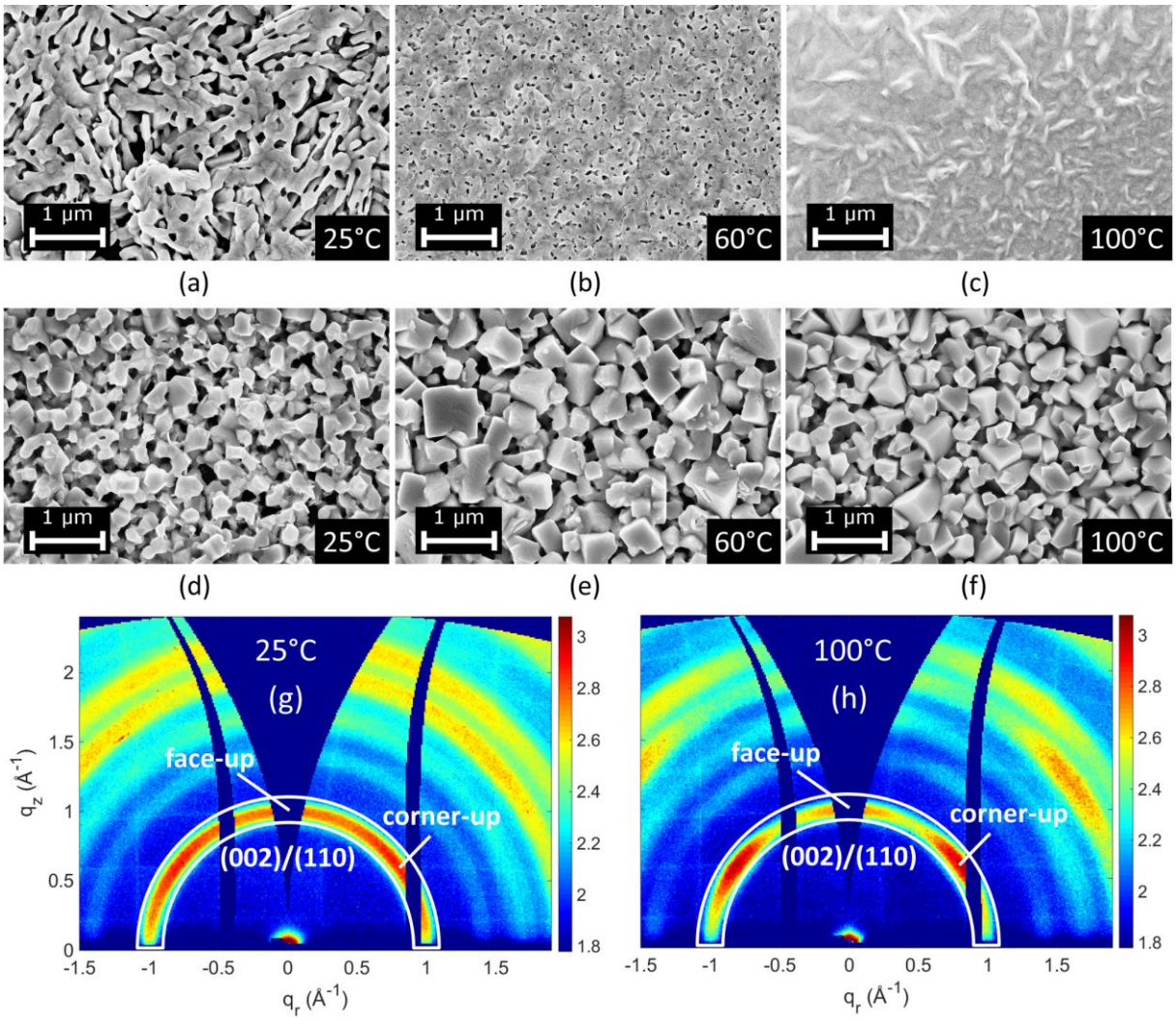

Figure 6. SEM top view images of (a)-(c) PbI_2 films spin-coated at 25 °C, 60 °C and 100 °C and (d)-(f) of the resulting MAPI films for 25 °C, 60 °C and 100 °C, respectively. GIWAXS data of the resulting MAPI films for (g) 25 °C and (h) 100 °C spin-coating temperature.

Figure 6 (a)-(f) shows SEM images of these films. The spin-coating temperature has a very large impact on the precursor film morphology. Spin-coating at a low temperature of 25 °C

results in a film that is strongly porous, the 60 °C temperature that is typically chosen results in a flat film with small pores roughly 50 nm in size, and spin-coating at high temperatures of 100 °C results in a dense film.

Both, a porous and a non-porous structure, can have advantages for the fabrication of homogeneous perovskite films. On the one hand, a porous structure makes it easier to convert the MAPI film and leaves space for the volume expansion during the conversion.[33] On the other hand, a structure that is too porous will leave gaps after conversion. Furthermore, a porous structure should also influence the prevalence of dissolution-recrystallization over in-situ conversion, as mentioned before. The resulting MAPI film morphology clearly shows why an elevated spin-coating temperature is preferable. When going from room temperature spin-coating to 60 °C spin-coating, the surface coverage becomes denser and the average size of larger crystallites doubles from around 250 nm to around 500 nm. The crystallites also become distinctly more cube-shaped. The change to even higher temperatures is smaller, though the sample spin-coated at 100 °C shows a larger number of smaller crystallites which could be a result of the mechanical reordering outlined in Section 2.2 and our earlier work.[27]

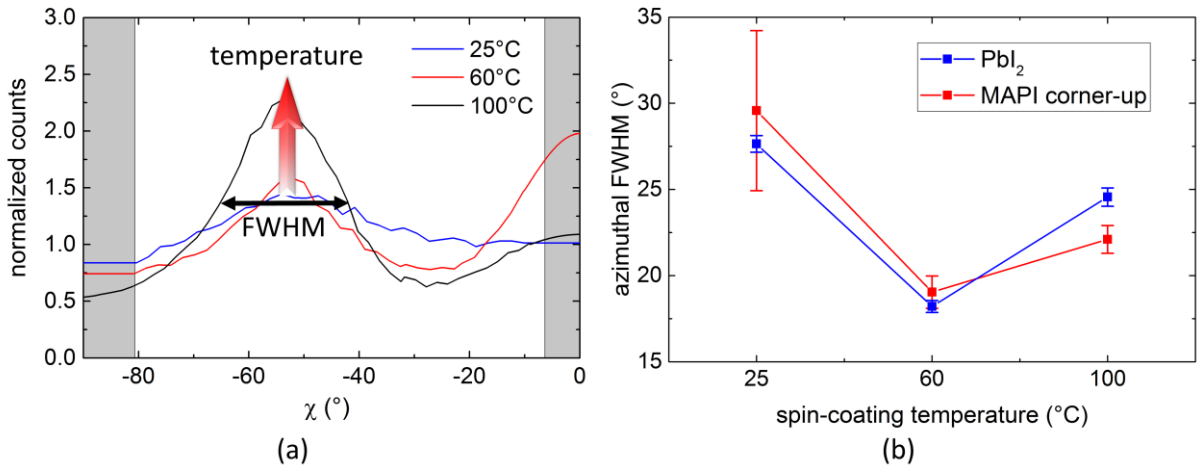

Figure 7. (a) Azimuthal integration of (002)/(110) peak for solution conversion samples spin-coated at different temperatures as indicated. (b) Azimuthal FWHM of the PbI_2 precursor orientation and the MAPI (202)/corner-up orientation.

The 2D data of the GIWAXS measurements on the 25 °C and the 100 °C MAPI samples is shown in Figure 6 (g) and 6 (h). The GIWAXS data for all samples studied in this section is shown in Figure S7 and azimuthal integrations of the (002)/(110) peak are shown in **Figure 7** (a). The lead iodide films all show (001) preferential orientation (cf. Figure S8) with some quantitative differences that are evaluated by the azimuthal FWHMs shown in Figure 7 (b). However, the resulting MAPI films show pronounced qualitative differences. All films have (202) preferential orientation, but the (002)/(110) orientation is absent from the 25 °C samples and only very weakly pronounced for the 100 °C sample. This preferential orientation is also evident from the more pronounced (202) peaks in XRD patterns (cf. Figure S6). The FWHM of the (202) orientations shown in Figure 7 (b) agree well with the FWHM of the respective lead iodide film preferential orientations. This indicates that the (202) orientation is indeed the result of an in-situ conversion process. We note that in comparison to Figure 2 (d) the crystal size is larger in Figure 6 (e) which is likely due to the different substrates used for the samples (TiO_2 and PEDOT:PSS). However, the orientations we find are the same for both PbI_2 and the resulting MAPI film, meaning that the conclusions of this paper are independent from the substrate, as expected based on our explanation of the orientations we find.

The comparison of azimuthal FHWM illustrates the need for GIWAXS for a quantitative evaluation of the orientation as XRD cannot distinguish between the overall prevalence and azimuthal width of a preferential orientation. However, the intensities seen in the GIWAXS cuts (Figure 7 (a)) coincide with the respective intensity of the (202) peak in XRD (Figure S6) and can be used for a qualitative explanation of the processes present:

The intensity of the (202) orientation increases with increasing temperature. Thereby, it increases with decreasing PbI_2 film porosity (cf. Figure 6 (a)-(c)). This agrees with our hypothesis of the (202) orientation being the result of an in-situ conversion process, since a dense, flat surface should suppress a dissolution of the film. The intensities of the (002)/(110)

orientation behave somewhat more erratically. It is stronger for the 60 °C sample than for the 100 °C sample, which agrees with our hypothesis of the origin of this orientation being a dissolution-recrystallization process. In this case, the porous surface of the 60 °C lead iodide sample should enhance the dissolution of the film compared to the dense surface morphology of the 100 °C film. However, the (002)/(110) orientation is almost completely absent from the 25 °C sample, illustrating that the (002)/(110) orientation is only a possible, but not a necessary result of a dissolution-recrystallization conversion. The absence of the (002)/(110) orientation from this sample can be explained by the fact that this preferential orientation should only be present relative to the surface on which the crystallization is taking place. Therefore, a crystallization in a very strongly porous film should not lead to an overall preferential orientation of crystallites in the film, which was demonstrated in literature by a comparison of preferential orientations for thin films produced on a flat surface and in a mesoporous scaffold.[34]

All in all, the correlation of the FWHM between the PbI_2 (001) orientation and the MAPI (202) orientation and the relation of their strength to the surface morphology prove that the (202) orientation is indeed the result of an in-situ conversion process.

3.2. The influence of chloride in the conversion solution

Employing chloride-containing precursors in the synthesis of perovskite films has been previously shown to improve the performance of the resulting solar cells.[22] On the other hand, it has been shown for a similar method that a high concentration of MAI is necessary for a strong dissolution of the PbI_2 film when a pure MAI conversion solution without chloride is used.[26] In the presented solution conversion method the rather low concentration should only lead to a comparatively small contribution of the dissolution-recrystallization mechanism. Since we linked the (002)/(110) orientation to a dissolution-recrystallization mechanism in the previous section, this implies a significant dissolution of the PbI_2 film for

the employed mixed halide solution. Here, we study the impact of chloride in the solution conversion mechanism on the morphology of the MAPI film and how its presence contributes to the relative prevalence of dissolution-recrystallization to in-situ conversion and the formation of different crystal orientations.

One known effect of chloride in the conversion solution is a larger size and a more cubic appearance of the individual crystallites.[22] A cubic shape has previously been associated with a dissolution-recrystallization mechanism, as it is thermodynamically favored. Thus, it forms when a MAPI crystallite grows directly from solution, but does not result from an in-situ conversion as the original PbI_2 crystallites have a different shape.[35]

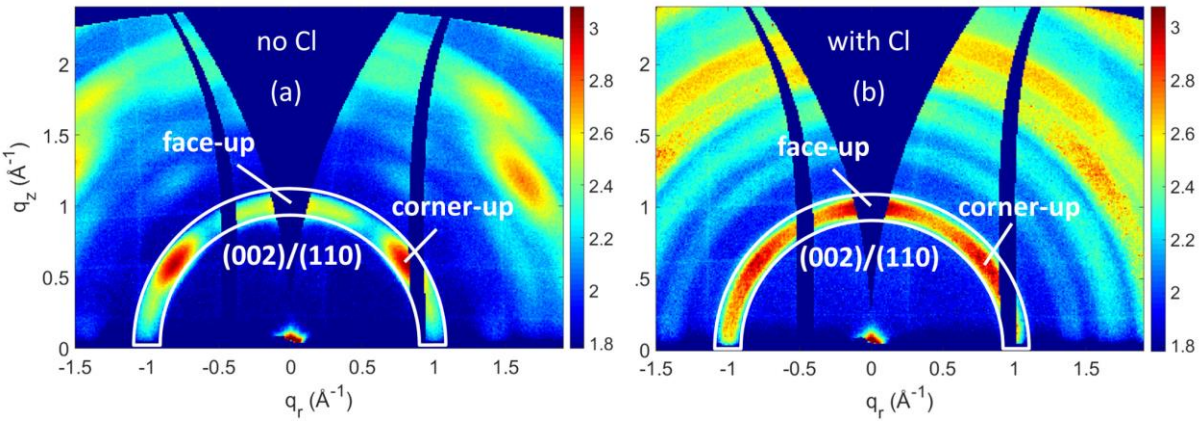

Figure 8. GIWAXS data for a solution conversion film spin-coated at 60 °C (a) without and (b) with chloride in the conversion solution.

The effect on the orientation is shown in **Figure 8**, where 2D GIWAXS data are shown for a SC film without chloride in the conversion solution in Fig. 8 (a) and for a SC film with chloride in the conversion solution in Fig. 8 (b). An azimuthal integration of the (002)/(110) peak is shown in Figure S10. The presence of chloride in the conversion solution leads to a strong decrease of the (202) preferential orientation and a strong increase of the (002)/(110) preferential orientation, which implies that chloride contributes to a dissolution-recrystallization-type conversion mechanism according to our hypothesis. This is to be

expected, since chloride is not incorporated into the structure to a significant degree and must thus facilitate a conversion process that is more complex than a simple in-situ conversion, e.g. by lowering the activation energy for the precursor-to-perovskite transition.[18]

In one-step methods which use chloride, an intermediate chloride phase appears during the film formation. This intermediate phase is then replaced by MAPI as it is more thermodynamically stable.[36,37] Therefore, it is plausible to speculate that the mechanism of the conversion of PbI_2 in two-step methods in the presence of chloride could involve an intermediate cubic $MAPbCl_3$ or $MAPbI_{3-x}Cl_x$ phase showing strong intrinsic (001) orientation, which is then converted to MAPI by a replacement of the halide ions similar to what is observed in one-step methods. [37,38] Chloride has previously been implied as increasing (001) orientation (face-up in cubic phase) in one-step methods.[36,39] This would explain why films converted in the presence of chloride show more (002)/(110) orientation (face-up in tetragonal phase). Since this process would require a dissolution of the PbI_6 octahedra, it can be considered a dissolution-recrystallization process, which agrees with the notion that (002)/(110) orientation is the result of this mechanism. In this regard, the role of chloride could be seen as the facilitation of the dissolution of the PbI_2 lead cage by providing an alternative conversion pathway with lower activation energy.[18]

By combining the evidence from the correlation of FWHM, the influence of surface morphology and the role of chloride, it can be concluded that the (202) orientation found in some two-step methods is indeed the result of an in-situ conversion process, while the (002)/(110) orientation is the result of a type of dissolution-recrystallization process.

4. Conclusion

Studying the orientation of perovskite films quantitatively by the aid of GIWAXS serves two purposes: As demonstrated in this investigation, it helps to understand the differences in film formation mechanics for different fabrication methods. In particular, for two-step processes, where the final orientation can be compared to the precursor film orientation, the GIWAXS analysis is complementary to SEM, which has been previously used to a large extent to study the formation of MAPI films.[26,35] Understanding these mechanisms could in turn lead to optimized processes that allow for better control of film morphology, including crystal size, density and orientation. These parameters are deemed beneficial for solar cell performance and likely influence each other. Specific orientations and large oriented domains have previously been reported as being important for achieving efficient charge transport and thereby large photocurrents.[20,29, 40,41] Reasons for this could include better charge transport between neighboring crystallites with similar orientation which likely reduces the prevalence of transport-hindering defects at the grain boundaries as well as different interactions between the crystal planes and the charge extraction layers.[42,43] As samples prepared on different substrates show essentially the same orientations, the implications of our study can be considered universal and independent of the substrate. This is not expected, as research from other groups (e.g. by G. Grancini et al.[44]) shows that surface roughness has a major influence on crystal growth when comparing planar and mesoporous TiO_2. Thus, studying the orientation of MAPI films can help to improve solar cell efficiencies of various planar architectures or other devices requiring efficient or anisotropic charge transport.

In summary, we compare the morphology of MAPI films prepared by a range of different one-step and two-step processes. They were chosen as representatives out of a variety of synthesis methods that produce high efficiency solar cells[11,14,22–24] but surprisingly exhibit very different morphologies. For the two investigated one-step methods, we do not find any significant preferential orientation. The three two-step methods start from a highly oriented

PbI_2 film in which the lead layers are lying parallel to the substrate. Despite the fixed orientation of the PbI_2 precursor film, we observe very different orientation distributions of the MAPI films after conversion. For a conversion in solution, we find strong (002)/(110) and (202) preferential orientation which would correspond to face-up and corner-up orientation for cube-shaped crystallites. For conversion by spin-coating MAI, we see weak face-up orientation, and for conversion in vapor, we observe no preferential orientation at all. Based on the comparison of the initial orientation and morphology of the precursor layer to the orientation and morphology of the resulting MAPI layer, we hypothesize that the corner-up preferential orientation of the solution conversion method is the result of an in-situ conversion mechanism, while the face-up orientation is based on a dissolution-recrystallization mechanism. Furthermore, due to the volume expansion of the PbI_2 film, mechanical reordering of crystallites takes place. In contrast, the lack of orientation of the evaporation method indicates a full dissolution of the film during conversion. Further evidence is given by our systematic study of the PbI_2 precursor film morphology. Varying the spin-coating temperature from 25 °C to 100 °C was found to produce PbI_2 films ranging from strongly porous to dense and flat which is found to influence the different crystal orientations in the resulting MAPI films. By correlating the width of the PbI_2 orientation to the width of the (202) MAPI orientation, the (202) orientation could be shown to be the result of an in-situ conversion process.

The presence of chloride in the conversion conclusion was found to enhance the (002)/(110) orientation at the expense of the (202) orientation, which is likely due to the formation of an (001) oriented intermediate phase.[18] Thus, the role of chloride in the film conversion for two-step methods is related to the facilitation of PbI_2 crystallite dissolution. We thus conclude that the (002)/(110) orientation is the result of a dissolution-recrystallization-type process. Overall, we provide tools for the systematic variation of PbI_2 film morphology and the resulting perovskite crystal orientation and a simple way to quickly characterize the

conversion mechanism of two-step methods by a comparison of precursor- and MAPI-film orientation.

5. Experimental Section

Sample preparation:

To obtain the required electrode pattern for solar cells, FTO coated glass substrates (7Ω/□, Pilkington) were etched with zinc powder and hydrochloric acid (2 M). The substrates were washed with an aqueous Alconox detergent solution, ethanol, acetone and isopropanol. Directly before the spin-coating of the next layer, they were cleaned in oxygen plasma for 10 min. TiO_2 was employed as the ETM. HCl (27.6 mM) in isopropanol was added dropwise to a titanium isopropoxide solution (0.43 M) in isopropanol. The resulting solution is stirred for 90 min. It is then spin-coated dynamically at 2000 rpm for 45 s and placed on a hotplate at 150°C for 5 min afterwards. The film is calcined at 500 °C for 1 hour.

Chlorobenzene method (CB):

First, stoichiometric amounts of PbI_2 and MAI (1:1 molar ratio, 1.25 M) were dissolved in anhydrous DMF. Subsequently, the perovskite precursor solution (75 µl) was dynamically spin-coated on the substrate at 5000 rpm. After a delay time of 4-5 s, anhydrous chlorobenzene (200 µl) was dripped as an antisolvent on the spinning sample. Finally, after a total spin-coating time of 30 s, the samples were immediately annealed at 100 °C for 10 min.

Lead acetate method (LA):

A solution of $Pb(CH_3COO)_2$ (1.5 M) and MAI (4.5 M) was prepared. The solution (100 µl) was spin-coated at 5000 rpm for 180 s. The samples were subsequently annealed at 100 °C for 2 min.

Solution conversion method (SC):

PbI_2 (394 mg/ml in Section 2 or 461 mg/ml in Section 3) was dissolved in DMF. Both the solution and the samples were kept at 60 °C prior to spin-coating for the standard sample in

Section 2 or kept at different temperatures ranging from 25 °C to 100 °C in Section 3. The solution (100 µl) was spin-coated dynamically at 3000 rpm for 15 s and afterwards annealed for 5 min. The samples were immersed in a MAI (9.5 mg/ml) / MACl (0.5 mg/ml) isopropanol solution at 60 °C for 10 minutes to convert the PbI_2 film to $MAPbI_3$. Afterwards, the samples were rinsed in isopropanol and quickly dried with a N_2 stream.

Evaporation method (EV):

PbI_2 (394 mg/ml) was dissolved in DMF. Both the solution and the samples were kept at 60 °C prior to spin-coating. The solution (100 µl) was spin-coated dynamically at 3000 rpm for 15 s and afterwards annealed for 5 min. The samples were placed in MAI vapor to convert them to MAPI for 2 hours. Afterwards, the samples were rinsed in isopropanol and quickly dried with a N_2 stream.

Interdiffusion method (ID):

PbI_2 (345.75 mg/ml) was dissolved in DMF. Both the solution and the samples were kept at 60 °C prior to spin-coating. The solution (100 µl) was spin-coated dynamically at 3000 rpm for 15 s. MAI (40 mg/ml) was dissolved in isopropanol. The solution (200 µl) was spin-coated at 3000 rpm for 30 s. The spin-coated films were annealed at 100 °C for 1 h.

Spiro:OMeTAD was employed as the HTM. Tert-butylpyridine (80 mM) and lithium bis(trifluoromethanesulphonyl)imide (25 mM) were added to a spiro-OMeTAD solution (7 vol%) in chlorobenzene. The solution was spin-coated at 1000 rpm for 45 s. Au was thermally evaporated on the sample as the top electrode.

The films investigated in Section 3 are prepared on glass slides which were cleaned as described for the samples on FTO. The samples are cleaned in oxygen plasma for 10 min. PEDOT:PSS (Clevios AI 4083, Ossila Ltd.) was spin-coated at 2500 rpm for 50 s and annealed at 140 °C for 10 min.

Sample Characterization:

X-ray diffraction (XRD) measurements were performed using a BRUKER D8 ADVANCE diffractometer with an 8 keV Cu-K_α X-ray source. Grazing-Incidence Wide Angle X-Ray Scattering (GIWAXS) measurements were performed using a Ganesha 300XL SAXS-WAXS with an 8 keV Cu-K_α X-ray source. Data was collected at an incident angle of 0.4 ° and a sample-detector distance of 106 mm with a Pilatus 300k detector. SEM measurements were performed using a Zeiss NVision40. UV-Vis measurements were performed using a PerkinElmer Lambda 650S with an integrating sphere. Profilometry measurements were performed using a Bruker DektakXT. The photovoltaic performance was measured with a Keithley 2400 SourceMeter under illumination by a Newport Oriel Sol2A solar simulator. The active area of the solar cells was defined to be 0.0831 cm^2 with a square metal aperture mask.

Supporting Information

Supporting Information is available from the Wiley Online Library or from the author.

Acknowledgements

The authors thank for funding from the Excellence Cluster “Nanosystems Initiative Munich” (NIM), the Center for NanoScience (CeNS) and the Bavarian Collaborative Research Project “Solar Technologies Go Hybrid” (SolTech). P.D. acknowledges support from the European Union through the award of a Marie Curie Intra-European Fellowship. Treatment of GIWAXS data was conducted using the software GIXSGUI provided free of charge by Advanced Photon Source, Argonne National Laboratory, USA. L. O. and J. S. contributed equally to this work.

Received: ((will be filled in by the editorial staff))
Revised: ((will be filled in by the editorial staff))
Published online: ((will be filled in by the editorial staff))

[1] A. Kojima, K. Teshima, Y. Shirai, T. Miyasaka, *J. Am. Chem. Soc.* **2009**, *131*, 6050.

[2] D. Bi, W. Tress, M. I. Dar, P. Gao, J. Luo, C. Renevier, K. Schenk, A. Abate, F. Giordano, J.-P. Correa Baena, J.-D. Decoppet, S. M. Zakeeruddin, M. K. Nazeeruddin, M. Gra tzel, and A. Hagfeldt, *Science Advances* **2016**, *2*, e1501170.

[3] Q. Dong, Y. Fang, Y. Shao, P. Mulligan, J. Qiu, L. Cao, J. Huang, *Science* **2015**, *347*, 967.

[4] S. D. Stranks, G. E. Eperon, G. Grancini, C. Menelaou, Alcocer, M. J. P., T. Leijtens, L. M. Herz, A. Petrozza, H. J. Snaith, *Science* **2013**, *342*, 341.

[5] C. C. Stoumpos, C. D. Malliakas, M. G. Kanatzidis, *Inorg. Chem.* **2013**, *52*, 9019.

[6] S. de Wolf, J. Holovsky, S.-J. Moon, P. Löper, B. Niesen, M. Ledinsky, F.-J. Haug, J.-H. Yum, C. Ballif, *J. Phys. Chem. Lett.* **2014**, *5*, 1035.

[7] C. Law, L. Miseikis, S. Dimitrov, P. Shakya-Tuladhar, X. Li, P. R. F. Barnes, J. Durrant, B. C. O'Regan, *Advanced materials* **2014**, *26*, 6268.

[8] J. Gong, S. B. Darling, F. You, *Energy Environ. Sci.* **2015**, *8*, 1953.

[9] T. C. Sum, N. Mathews, *Energy Environ. Sci.* **2014**, *7*, 2518.

[10] G. E. Eperon, V. M. Burlakov, P. Docampo, A. Goriely, H. J. Snaith, *Adv. Funct. Mater.* **2014**, *24*, 151.

[11] M. Xiao, F. Huang, W. Huang, Y. Dkhissi, Y. Zhu, J. Etheridge, A. Gray-Weale, U. Bach, Y.-B. Cheng, L. Spiccia, *Angew. Chem. Int. Ed.* **2014**, *53*, 9898.

[12] H. Hu, D. Wang, Y. Zhou, J. Zhang, S. Lv, S. Pang, X. Chen, Z. Liu, N. P. Padture, G. Cui, *RSC Adv.* **2014**, *4*, 28964.

[13] D. Liu, J. Yang, T. L. Kelly, *J. Am. Chem. Soc.* **2014**, *136*, 17116.

[14] Z. Xiao, C. Bi, Y. Shao, Q. Dong, Q. Wang, Y. Yuan, C. Wang, Y. Gao, J. Huang, *Energy Environ. Sci.* **2014**, *7*, 2619.

[15] D. Bi, A. M. El-Zohry, A. Hagfeldt, G. Boschloo, *ACS Appl. Mater. Interfaces* **2014**, *6*, 18751.

[16] A. Hexemer, P. Müller-Buschbaum, *IUCrJ* **2015**, *2*, 106.

[17] K. W. Tan, D. T. Moore, M. Saliba, H. Sai, L. A. Estroff, T. Hanrath, H. J. Snaith, U. Wiesner, *ACS Nano* **2014**, *8*, 4730.

[18] D. T. Moore, H. Sai, K. W. Tan, D.-M. Smilgies, W. Zhang, H. J. Snaith, U. Wiesner, L. A. Estroff, *J. Am. Chem. Soc.* **2015**, *137*, 2350.

[19] E. L. Unger, A. R. Bowring, C. J. Tassone, V. L. Pool, A. Gold-Parker, R. Cheacharoen, K. H. Stone, E. T. Hoke, M. F. Toney, M. D. McGehee, *Chem. Mater.* **2014**, *26*, 7158.

[20] M. Saliba, K. W. Tan, H. Sai, D. T. Moore, T. Scott, W. Zhang, L. A. Estroff, U. Wiesner, H. J. Snaith, *J. Phys. Chem. C* **2014**, *118*, 17171.

[21] M. A. Ruderer, S. Guo, R. Meier, H.-Y. Chiang, V. Körstgens, J. Wiedersich, J. Perlich, S. V. Roth, P. Müller-Buschbaum, *Adv. Funct. Mater.* **2011**, *21*, 3382.

[22] P. Docampo, F. C. Hanusch, S. D. Stranks, M. Döblinger, J. M. Feckl, M. Ehrensperger, N. K. Minar, M. B. Johnston, H. J. Snaith, T. Bein, *Adv. Energy Mater.* **2014**, *4*, 1400355.

[23] Q. Chen, H. Zhou, Z. Hong, S. Luo, H.-S. Duan, H.-H. Wang, Y. Liu, G. Li, Y. Yang, *J. Am. Chem. Soc.* **2014**, *136*, 622.

[24] W. Zhang, M. Saliba, D. T. Moore, S. K. Pathak, M. T. Hörantner, T. Stergiopoulos, S. D. Stranks, G. E. Eperon, J. A. Alexander-Webber, A. Abate, A. Sadhanala, S. Yao, Y. Chen, R. H. Friend, L. A. Estroff, U. Wiesner, H. J. Snaith, *Nat Comms* **2015**, *6*, 6142.

[25] J. L. Baker, L. H. Jimison, S. Mannsfeld, S. Volkman, S. Yin, V. Subramanian, A. Salleo, A. P. Alivisatos, M. F. Toney, *Langmuir* **2010**, *26*, 9146.

[26] Y. Fu, F. Meng, M. B. Rowley, B. J. Thompson, M. J. Shearer, D. Ma, R. J. Hamers, J. C. Wright, S. Jin, *J. Am. Chem. Soc.* **2015**, *137*, 5810.

[27] J. Schlipf, P. Docampo, C. J. Schaffer, V. Körstgens, L. Bießmann, F. Hanusch, N. Giesbrecht, S. Bernstorff, T. Bein, P. Müller-Buschbaum, *J. Phys. Chem. Lett.* **2015**, *6*, 1265.

[28] C. Zuo, L. Ding, *Nanoscale* **2014**, *6*, 9935.

[29] L. Huang, Z. Hu, G. Yue, J. Liu, X. Cui, J. Zhang, Y. Zhu, *Phys. Chem. Chem. Phys.* **2015**, *17*, 22015.

[30] T. Zhang, M. Yang, Y. Zhao, K. Zhu, *Nano Lett.* **2015**, *15*, 3959.

[31] P. Pistor, J. Borchert, W. Fränzel, R. Csuk, R. Scheer, *J. Phys. Chem. Lett.* **2014**, *5*, 3308.

[32] H.-S. Ko, J.-W. Lee, N.-G. Park, *J. Mater. Chem. A* **2015**, *3*, 8808.

[33] H. Zheng, W. Wang, S. Yang, Y. Liu, J. Sun, *RSC Adv* **2016**, *6*, 1611.

[34] W. Huang, F. Huang, E. Gann, Y.-B. Cheng, C. R. McNeill, *Adv. Funct. Mater.* **2015**, *25*, 5529.

[35] S. Yang, Y. C. Zheng, Y. Hou, X. Chen, Y. Chen, Y. Wang, H. Zhao, H. G. Yang, *Chem. Mater.* **2014**, *26*, 6705.

[36] S. T. Williams, F. Zuo, C.-C. Chueh, C.-Y. Liao, P.-W. Liang, A. K.-Y. Jen, *ACS Nano* **2014**, *8*, 10640.

[37] A. Binek, I. Grill, N. Huber, K. Peters, A. G. Hufnagel, M. Handloser, P. Docampo, A. Hartschuh, T. Bein, *Chem. Asian J* **2016**, *11*, 1119

[38] D. P. Nenon, J. A. Christians, L. M. Wheeler, J. L. Blackburn, E. M. Sanehira, B. Dou, M. L. Olsen, K. Zhu, J. J. Berry, and J. M. Luther, *Energy Environ. Sci*. **2016**, *9*, 2072–2082.

[39] Y. Zhao, K. Zhu, *J. Phys. Chem. C* **2014**, *118*, 9412.

[40] P. Docampo, F. C. Hanusch, N. Giesbrecht, P. Angloher, A. Ivanova, T. Bein, *APL Mater.* **2014**, *2*, 81508.

[41] N. Giesbrecht, J. Schlipf, L. Oesinghaus, A. Binek, T. Bein, P. Müller-Buschbaum, and P. Docampo, *ACS Energy Lett.* **2016**, *1*, 150–154.

[42] A. Torres, Rego, Luis G. C., *J. Phys. Chem. C* **2014**, *118*, 26947.

[43] J. Feng, B. Xiao, *J. Phys. Chem. Lett.* **2014**, *5*, 1278.

[44] G. Grancini, S. Marras, M. Prato, C. Giannini, C. Quarti, F. de Angelis, M. de Bastiani, G. E. Eperon, H. J. Snaith, L. Manna, and A. Petrozza, *J. Phys. Chem. Lett.* **2014,** *5*, 3836.

The origin of orientation in MAPI films produced by sequential deposition methods is investigated by grazing-incidence wide-angle X-ray scattering. An overview over morphologies produced by typical fabrication methods is given, and the morphology and orientation of the precursor and the resulting perovskite film is shown to be linked in different ways depending on the conversion method.

perovskite film structure, grazing-incidence wide-angle X-ray scattering, sequential deposition, the role of chloride, conversion mechanism

Lukas Oesinghaus, Johannes Schlipf, Nadja Giesbrecht, Lin Song, Yinghong Hu, Thomas Bein, Pablo Docampo *, Peter Müller-Buschbaum *

Towards Tailored Film Morphologies: The Origin of Crystal Orientation in Hybrid Perovskite Thin Films

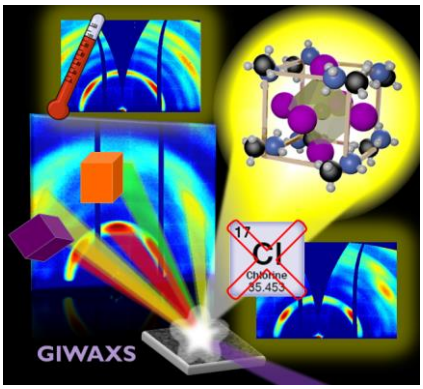

Figute 1

Click here to access/download

Production Data

Figure 1.tif

Figure 2

Figure 3


Click here to access/download
Production Data
Figure 3 new.tif

Figure 4

Figure 5

Figure 6


Click here to access/download
Production Data
Figure 6 new.tif

Figure 7

Figure 8


Click here to access/download
Production Data
Figure 8 new.tif